INTERNATIONAL JOURNAL OF NUMERICAL MODELLING: ELECTRONIC NETWORKS, DEVICES AND FIELDS
Int. J. Numer. Model. 2007; **21**:29–42
Published online 24 September 2007 in Wiley InterScience (www.interscience.wiley.com). DOI: 10.1002/jnm.662

FVTD—integral equation hybrid for Maxwell's equations

Dmitry K. Firsov and Joe LoVetri*,†

Department of Electrical and Computer Engineering, University of Manitoba, Winnipeg, MB, Canada R3T 5V6

SUMMARY

A new hybrid finite-volume time-domain integral equation (FVTD/IE) algorithm for the solution of Maxwell's Equations on unstructured meshes of arbitrary flat-faceted volume elements is presented. A time-domain IE-based numerical algorithm is applied on the boundary of the computational domain to determine the incoming fluxes for the boundary facets of the mesh. This method is a global grid-truncation technique similar to the method previously introduced for the finite-difference time-domain scheme by Ziolkowski *et al*. The three main advantages of this IE truncation method are that (1) it allows geometrical objects to be located (almost) arbitrarily close to the mesh boundaries without compromising the physics of the problem, (2) it couples the physics of unconnected meshes so that distant scatterers can be surrounded by their own local mesh, thus reducing total mesh size, and (3) the same IE formulation can be used to compute electromagnetic field values at points outside the mesh. Currently, the main disadvantage is that an acceleration scheme for performing the IE update, which requires integrating field components on an interior surface at a retarded time, is not available. Computational results are presented for the scattering from a perfectly electrical conducting sphere and compared numerically with the analytic time-domain solution as well as the solution obtained using a large spherical outer mesh boundary with local absorbing boundary conditions. Results are excellent and show almost no reflections from the mesh boundary even when the observation point is located close to the corner of the cubically shaped outside mesh boundary. Results are also presented and validated for the scattering from two objects that are contained inside their own unconnected meshes. Copyright © 2007 John Wiley & Sons, Ltd.

Received 8 March 2007; Revised 9 August 2007; Accepted 10 August 2007

KEY WORDS: finite-volume time-domain; FVTD; Maxwell's equations; integral equation truncation scheme

1. INTRODUCTION

The *standard* finite-difference time-domain (FDTD) method is a very popular method for computational electromagnetics because of its ease of implementation, but it requires that

*Correspondence to: Joe LoVetri, Department of Electrical and Computer Engineering, University of Manitoba, Winnipeg, MB, Canada R3T 5V6.
†E-mail: lovetri@ee.umanitoba.ca

Contract/grant sponsor: Defence Research and Development Canada
Contract/grant sponsor: NSERC

curved geometries be approximated by 'stair-stepping' the boundaries and the electromagnetic field components are interlaced in space and time [1]. On the other hand, the finite-volume technique is a standard technique used in computational fluid dynamics (CFD) [2], which can be implemented on unstructured grids and therefore is better suited to modelling curved geometries. Several finite-volume time-domain (FVTD) formulations for Maxwell's equations are available, but a recently developed version has provided good results for a wide variety of problems [3, 4]. This method collocates all the field components at the centre of each finite volume and is implemented on unstructured meshes. It is a *characteristic-based* FVTD scheme that uses a two-step second-order upwinding scheme in the time domain. It also uses a second-order accurate MUSCL-type scheme to interpolate the fluxes at the finite-volume facets [5, 6]. Recently, we have reported the extension of this method using higher-order spatial interpolation techniques [7, 8]. In [9], a new stability criterion for these methods has been reported which relaxes the overly conservative criterion that was provided in [3].

In this paper we present the use of a time-domain integral equation (IE)-based algorithm to truncate the boundary of the FVTD mesh. This IE technique is similar to the one that was first introduced for the FDTD algorithm by Ziolkowski *et al*. called the *Global Lookback Lattice Scheme* [10]. Implementing such a truncation algorithm for the characteristic-based FVTD scheme is tricky because of the flux splitting at the finite-volume cell boundaries. The key idea in incorporating the IE truncation into the FVTD algorithm is to use the IE to update only the incoming fluxes on the boundary facets (as opposed to using it to update the total field values). Here, we provide details of the hybrid FVTD/IE algorithm for the FVTD scheme using MUSCL-type interpolation.

In Section 2 we give a detailed overview of the theory behind the FVTD method as implemented in our code. In the following section we describe the IE formulation at the boundary of our mesh. In Section 4 we compare computational results with the analytic solution for the perfectly electrical conducting (PEC)-sphere scattering, as well as for the test case of transient scattering from two PEC cubes located in separate FVTD meshes.

2. FVTD FOR MAXWELL'S EQUATIONS

The FVTD algorithm is usually applied to physical phenomena that are governed by a *conservation law*. The FVTD method for solving electromagnetic problems considers all of the electric and magnetic field components as components of a solution vector $\mathbf{u} = [\mathbf{E}\ \mathbf{H}]^{\mathrm{T}}$, and then casts Maxwell's equations in a conservation law form. Following a procedure similar to that given in [3], starting from Maxwell's two curl equations in a lossy, isotropic, homogeneous medium,

$$\begin{aligned} \varepsilon\partial_t\mathbf{E} - \nabla\times\mathbf{H} + \sigma\mathbf{E} &= -\mathbf{J} \\ \mu\partial_t\mathbf{H} + \nabla\times\mathbf{E} &= 0 \end{aligned} \tag{1}$$

we employ the matrix operator

$$\mathbf{S}(\mathbf{x})\mathbf{b} = \begin{bmatrix} 0 & -x_3 & x_2 \\ x_3 & 0 & -x_1 \\ -x_2 & x_1 & 0 \end{bmatrix} \begin{bmatrix} b_1 \\ b_2 \\ b_3 \end{bmatrix} = \mathbf{x}\times\mathbf{b} \tag{2}$$

DOI: 10.1002/jnm

by which the curl of a vector can be expressed in terms of the divergence of a matrix operating on the vector

$$\nabla \times \mathbf{x} = (\operatorname{div} \mathbf{S}(\mathbf{x}))^{\mathrm{T}} = \begin{bmatrix} \partial_2 x_3 - \partial_3 x_2 \\ -\partial_1 x_3 + \partial_3 x_1 \\ \partial_1 x_2 - \partial_2 x_1 \end{bmatrix} \tag{3}$$

In terms of this new operator, Maxwell's equations can be written as

$$\varepsilon \partial_t \mathbf{E} - (\operatorname{div} \mathbf{S}(\mathbf{H}))^{\mathrm{T}} + \sigma \mathbf{E} = -\mathbf{J}$$

$$\mu \partial_t \mathbf{H} + (\operatorname{div} \mathbf{S}(\mathbf{E}))^{\mathrm{T}} = \mathbf{0} \tag{4}$$

or, even more succinctly as

$$\partial_t \mathbf{u} + \boldsymbol{\alpha}^{-1} \mathbf{K}\mathbf{u} = \boldsymbol{\alpha}^{-1}(\mathbf{G} + \mathbf{B}\mathbf{u}) \tag{5}$$

where

$$\boldsymbol{\alpha} = \begin{bmatrix} \varepsilon \mathbf{I} & \mathbf{0} \\ \mathbf{0} & \mu \mathbf{I} \end{bmatrix}, \quad \mathbf{K}\mathbf{u} = \begin{bmatrix} -\nabla \times \mathbf{H} \\ \nabla \times \mathbf{E} \end{bmatrix}, \quad \mathbf{B} = \begin{bmatrix} -\boldsymbol{\sigma} & \mathbf{0} \\ \mathbf{0} & \mathbf{0} \end{bmatrix}, \quad \mathbf{G} = \begin{bmatrix} -\mathbf{J} \\ \mathbf{0} \end{bmatrix} \tag{6}$$

where $\mathbf{I}$ is the identity matrix. Integrating (5) over an element denoted by T_i with boundary ∂T_i and using the divergence theorem to convert the integral over volume to integrals over the surface we arrive at

$$\int_{T_i} \partial_t \mathbf{u} \, \mathrm{d}\mathbf{x} + \int_{\partial T_i} \boldsymbol{\alpha}^{-1} \mathbf{A}(\hat{\mathbf{n}}) \mathbf{u} \, \mathrm{d}\mathbf{s} = \int_{T_i} \boldsymbol{\alpha}^{-1} \mathbf{G} \, \mathrm{d}\mathbf{x} + \int_{T_i} \boldsymbol{\alpha}^{-1} \mathbf{B}\mathbf{u} \, \mathrm{d}\mathbf{x} \tag{7}$$

where matrix $\mathbf{A}(\hat{\mathbf{n}})$ is defined by

$$\mathbf{A}(\hat{\mathbf{n}}) = \begin{bmatrix} \mathbf{0} & -\mathbf{S}(\hat{\mathbf{n}}) \\ \mathbf{S}(\hat{\mathbf{n}}) & \mathbf{0} \end{bmatrix} \tag{8}$$

and $\hat{\mathbf{n}}$ denotes the outward normal to the volume surface ∂T_i. The vector quantity $\mathbf{A}(\hat{\mathbf{n}})\mathbf{u}$ is referred to as the flux through the surface ∂T_i (a few more details can be found in [8]).

We now associate with each cell a value of the average of the generalized solution vector $\mathbf{u}_i$ located at the barycentre $\mathbf{x}_i$ of element T_i. This is calculated as

$$\mathbf{u}_i = \frac{1}{\mu(T_i)} \int_{T_i} \mathbf{u}(\mathbf{x}) \, \mathrm{d}\mathbf{x} = \mathbf{u}(\mathbf{x}_i) + O(||\Delta \mathbf{x}||^2) \tag{9}$$

where $\mu(T_i)$ gives the volume of element T_i, and $||\Delta \mathbf{x}||^2$ scales with the size of the element. To perform *flux splitting*, we first define $\tilde{\mathbf{A}}(\hat{\mathbf{n}}) = \boldsymbol{\alpha}^{-1} \mathbf{A}(\hat{\mathbf{n}})$ which can be decomposed as a sum of matrices with positive and negative eigenvalues. It can be shown that $\tilde{\mathbf{A}}(\hat{\mathbf{n}})$ has six eigenvalues given by $\mathbf{L} = \operatorname{diag}\{0, 0, v, v, -v, -v\}$, where $v = 1/\sqrt{\varepsilon\mu}$, and can be decomposed as

$$\tilde{\mathbf{A}}(\hat{\mathbf{n}}) = \tilde{\mathbf{A}}(\hat{\mathbf{n}})^{+} + \tilde{\mathbf{A}}(\hat{\mathbf{n}})^{-} \tag{10}$$

where

$$\tilde{\mathbf{A}}(\hat{\mathbf{n}})^{+} = \frac{1}{2} \begin{bmatrix} -v\mathbf{S}(\hat{\mathbf{n}})^2 & -\varepsilon^{-1}\mathbf{S}(\hat{\mathbf{n}}) \\ \mu^{-1}\mathbf{S}(\hat{\mathbf{n}}) & -v\mathbf{S}(\hat{\mathbf{n}})^2 \end{bmatrix} \quad \text{and} \quad \tilde{\mathbf{A}}(\hat{\mathbf{n}})^{-} = \frac{1}{2} \begin{bmatrix} v\mathbf{S}(\hat{\mathbf{n}})^2 & -\varepsilon^{-1}\mathbf{S}(\hat{\mathbf{n}}) \\ \mu^{-1}\mathbf{S}(\hat{\mathbf{n}}) & v\mathbf{S}(\hat{\mathbf{n}})^2 \end{bmatrix} \tag{11}$$

DOI: 10.1002/jnm

To compute the value of the surface integral associated with a volume T_i in (7) we require knowledge of the flux $\tilde{\mathbf{A}}(\hat{\mathbf{n}})\mathbf{u}$ on all the facets of the boundary ∂T_i. To determine the flux, we let $\mathbf{u}^*$ denote the solution vector on the internal side of each facet of ∂T_i while using $\mathbf{u}^{**}$ to denote the solution vector just to the outside of each such facet. These are obtained by interpolation centred on the relevant side of each facet. In this paper, all interpolations are performed using the MUSCL scheme [3]. As shown in our previous paper [8], for facets separating volumes having different material properties, the flux can be concisely represented as

$$\tilde{\mathbf{A}}(\hat{\mathbf{n}})\mathbf{u} = \tilde{\mathbf{A}}(\hat{\mathbf{n}})^{+}\mathbf{u}^{*} + \tilde{\mathbf{A}}(\hat{\mathbf{n}})^{-}\mathbf{u}^{**} \tag{12}$$

where

$$\mathbf{T}_i = 2\begin{bmatrix} Y_k(Y_i + Y_k)^{-1}\mathbf{I} & \mathbf{0} \\ \mathbf{0} & Z_k(Z_i + Z_k)^{-1}\mathbf{I} \end{bmatrix}, \quad \mathbf{T}_k = 2\begin{bmatrix} Y_i(Y_i + Y_k)^{-1}\mathbf{I} & \mathbf{0} \\ \mathbf{0} & Z_i(Z_i + Z_k)^{-1}\mathbf{I} \end{bmatrix} \tag{13}$$

$\mathbf{I} \in R^{3\times 3}$is the identity matrix and $Z = Y^{-1}$ is the impedance. For PEC facets it can be shown that the linear operation of $\mathbf{A}(\hat{\mathbf{n}})$ on $\mathbf{u}$ becomes $\mathbf{A}(\hat{\mathbf{n}}) = \boldsymbol{\alpha}_i\mathbf{T}^{pc}\tilde{\mathbf{A}}(\hat{\mathbf{n}})^{+}\mathbf{u}^{*}$, where

$$\mathbf{T}^{pc} = \begin{bmatrix} \mathbf{2I} & \mathbf{0} \\ \mathbf{0} & \mathbf{0} \end{bmatrix} \tag{14}$$

In the scattered field formulation the flux at a PEC facet is given by

$$\mathbf{A}(\hat{\mathbf{n}})\mathbf{u}^{s} = \boldsymbol{\alpha}_{\mathbf{i}}\mathbf{T}^{pc}\tilde{\mathbf{A}}(\hat{\mathbf{n}})^{+}\mathbf{u}^{s*} - \mathbf{2}\tilde{\mathbf{A}}(\hat{\mathbf{n}})^{-}\mathbf{G}^{s*} \tag{15}$$

where $\mathbf{G}^{s*} = [\mathbf{E}^{i}\ \ \mathbf{0}]^{*\mathrm{T}}$ represents a source term.

For a mesh comprising N elements we may write the flux integration at each element in the vector form as

$$\left[\frac{1}{V_1}\left(\int_{\partial T_1}\boldsymbol{\alpha}^{-1}\mathbf{A}(\hat{\mathbf{n}})\mathbf{u}\,\mathrm{d}\mathbf{s}\right)^{\mathrm{T}}\frac{1}{V_2}\left(\int_{\partial T_2}\boldsymbol{\alpha}^{-1}\mathbf{A}(\hat{\mathbf{n}})\mathbf{u}\,\mathrm{d}\mathbf{s}\right)^{\mathrm{T}}\cdots\frac{1}{V_{\mathrm{N}}}\left(\int_{\partial T_{\mathrm{N}}}\boldsymbol{\alpha}^{-1}\mathbf{A}(\hat{\mathbf{n}})\mathbf{u}\,\mathrm{d}\mathbf{s}\right)^{\mathrm{T}}\right]^{\mathrm{T}} \approx \mathbf{LU} \tag{16}$$

where $\mathbf{U} = [\mathbf{u}_1^{\mathrm{T}}\ \mathbf{u}_2^{\mathrm{T}}\ldots\mathbf{u}_N^{\mathrm{T}}]^{\mathrm{T}}$ is the vector of unknowns in each element and where the division by volume V_i arises due to the barycentric averaging of $\mathbf{u}_i$. Using the result of (16) in the volume integration of (5) gives

$$\partial_t\mathbf{U} + \mathbf{LU} = \mathbf{F} \tag{17}$$

where the time derivative is taken element-by-element over $\mathbf{U}$ and where $\mathbf{F}$ is a source term with each element i of $\mathbf{F}$ representing the right-hand side of (5) integrated over the ith volume.

Having organized the flux integration into a matrix–vector product over the entire computational space, it remains to discretely approximate the time derivative in (17). For the results presented herein, we use a standard second-order accurate predictor–corrector scheme given as

$$\begin{aligned} \mathbf{U}^{(n+1/2)} &= \mathbf{U}^{(n)} - \frac{\Delta t}{2}\mathbf{L}\mathbf{U}^{(n)} \\ \mathbf{U}^{(n+1)} &= \mathbf{U}^{(n)} - \frac{\Delta t}{2}\mathbf{L}\mathbf{U}^{(n+1/2)} \end{aligned} \tag{18}$$

DOI: 10.1002/jnm

Being an explicit time-integration scheme, there is a time-step limitation for retaining stability. The computational results in this paper are calculated using the new time-step stability criterion described in [9].

3. MUSCL INTERPOLATORY SCHEME AND ABSORBING BOUNDARY CONDITIONS

For the calculation of fluxes at the element facets we use a MUSCL-type interpolation scheme (as was used in [3]). The MUSCL scheme is a well-known scheme that was devised for CFD [5]. The scheme is based on Taylor interpolation and is easy to describe for a scalar function $\mathbf{u}(\mathbf{r})$. Start by first approximating the function $\mathbf{u}(\mathbf{r})$, for all values r on each element T_i of computational domain, by

$$\mathbf{u}(\mathbf{r}) = \mathbf{u}_i + (\mathbf{r} - \mathbf{r}_i) \cdot \nabla \mathbf{u}(\mathbf{r}_i) + O(||\mathbf{r} - \mathbf{r}_i||^2) \tag{19}$$

Here, although the gradient may be approximated with first-order accuracy, the dot product of the gradient with $\mathbf{r} - \mathbf{r}_i$ produces a second-order accurate interpolation scheme. With the following identity, based on the gradient theorem, we obtain

$$\int_{T_i} \nabla \mathbf{u}(\mathbf{r}) \, \mathrm{d}V = \int_{\partial T_i} \hat{\mathbf{n}} \mathbf{u}(\mathbf{r}) \, \mathrm{d}S = \sum_{k=1}^{m_i} S_i(k) \hat{\mathbf{n}}_i(k) \mathbf{u}_i(k) \tag{20}$$

where $S_i(k)$ and $\hat{\mathbf{n}}_i(k)$ represent the area of and normal vector to the kth facet for the ith volume. On a single flat facet, $\partial T_i(k)$, of the element i we define the average value of the solution for the facet as

$$\mathbf{u}_i(k) = \frac{1}{S_i(k)} \int_{\partial T_i(k)} \mathbf{u}(\mathbf{r}) \, \mathrm{d}S \tag{21}$$

This average value on the facets of each tetrahedral, $\mathbf{u}_i(k)$, can be approximated with first- or second-order accuracy by interpolating the solution calculated at the barycentres of the neighbouring elements that share that facet. For cases that we know the solution on the facet, e.g. from PEC boundary conditions, we can use the known value instead of interpolation. From these interpolated average values, we can calculate the average of the gradient by dividing (20) by the volume. This average of the gradient will be a second-order accurate approximation to the gradient at the barycentre of the element.

For the gradient computation of an element having a facet on an exterior surface with absorbing boundary conditions, we can use the idea that the incoming flux to the computational domain is equal to zero. As a second-order approximation the value on a facet which is on an absorbing boundary can be set equal to the solution value at the barycentre of the element. Alternatively, higher-order interpolation formulas can be used based on calculated values on the interior of the mesh. Although we have implemented these, they are not considered in this paper. It has been found that the second-order interpolation works well if the outside mesh boundary is chosen to be a large sphere.

Thus, for purposes of this paper we can provide a simple formula for calculating the gradient at the barycentre of each finite volume:

$$\nabla \mathbf{u}(\mathbf{r}_i) \approx \frac{1}{V_i} \sum_{k=1}^{m_i} S_i(k) \hat{\mathbf{n}}_i(k) (\beta_i^k \mathbf{u}_i + (1 - \beta_i^k) \mathbf{u}_{i_k}) \tag{22}$$

DOI: 10.1002/jnm

where for absorbing boundary conditions $\beta_i^k = 1$, when we know the value $\mathbf{w}_{i_k}$ on the facet $\mathbf{u}_{i_k} = \mathbf{w}_{i_k}$ and $\beta_i^k = 0$. For the case when there exists element T_{i_k} sharing the kth facet we can use the $\mathbf{u}_{i_k}$ value from the barycentre of the neighbouring element and $\beta_i^k = |\hat{\mathbf{n}}_i(k) \cdot (\mathbf{r}_{i_k} - \mathbf{r}_{ik})|/|\hat{\mathbf{n}}_i(k) \cdot (\mathbf{r}_i - \mathbf{r}_{i_k})|$, where $\mathbf{r}_{ik}$ is the position vector of the barycentre of the kth facet of the ith element, and $\mathbf{r}_{ik}$ is the position vector of neighbouring element's barycentre.

4. INTEGRAL EQUATION BOUNDARY CONDITIONS

We now consider the representation of an electromagnetic field in terms of its values on a closed surface in the same way as was done by Ziolkowski *et al.* [10]. The physical problem space is first divided into two separate volumes bounded by surfaces Σ and S as shown in Figure 1. The surface Σ bounds the whole computational region of interest and we assume that outside of the surface S is free space. The region of interest bounded by S will contain all sources as well as medium inhomogeneities. Now suppose we consider an observation point $\mathbf{r}$ which lies in the free-space region outside of S and consider a point s on the surface S. The electric and magnetic fields at $\mathbf{r}$ and at time t can be represented in terms of field values on S at a retarded time by integrating these field values at all such points s on S. The final expression can be written as [10]

$$\mathbf{E}(t,\mathbf{r}) = \int_S \frac{\theta(t-\tau)}{4\pi R}\{\hat{\mathbf{n}} \times [\mathbf{E} + \tau\partial_t \mathbf{E}] \times \mathbf{R} + (\hat{\mathbf{n}} \cdot [\mathbf{E} + \tau\partial_t \mathbf{E}])\mathbf{R} - \hat{\mathbf{n}} \times [\mu_0 \partial_t \mathbf{H}]\}\, \mathrm{d}S$$

$$\mathbf{H}(t,\mathbf{r}) = \int_S \frac{\theta(t-\tau)}{4\pi R}\{\hat{\mathbf{n}} \times [\mathbf{H} + \tau\partial_t \mathbf{H}] \times \mathbf{R} + (\hat{\mathbf{n}} \cdot [\mathbf{H} + \tau\partial_t \mathbf{H}])\mathbf{R} + \hat{\mathbf{n}} \times [\varepsilon_0 \partial_t \mathbf{E}]\}\, \mathrm{d}S \qquad (23)$$

where $\partial_t = \partial/\partial t$, $\theta(t)$ is the step function and $\mathbf{R} = (\mathbf{r} - \mathbf{s})/R^2$, where the distance from the source point to the observation point is given by $R = ||\mathbf{r} - \mathbf{s}||$. Here, we let $\tau = R/c$ denote the *retarded time*, and the notation $[f] = f(\mathbf{s}, t_k)$ is used to denote the value of function f at location s evaluated at the retarded time.

These can be used to truncate the FVTD mesh as follows (see Figure 1). To determine the field value at a point on the outer mesh boundary, Σ, instead of using local absorbing boundary conditions, we use the IE evaluated using FVTD computed field values on an internal closed

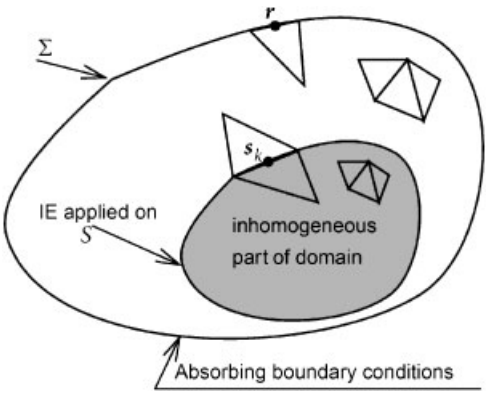

Figure 1. Coupling of IE surface to FVTD grid.

DOI: 10.1002/jnm

surface S. The surface S is made up of finite-volume facets. We also use the IE to compute the solution at any observation points of interest inside or outside of the computational domain.

We now give a brief description of how the integral is computed on S. After discretization of the computational domain, using tetrahedrals in our case, the surface S can be represented as a union of N_S flat surface facets S_k:

$$S = \bigcup_{k=1}^{N_S} S_k$$

Hence, the integrals of Equation (23) can be approximated as a sum of influences from all these facets S_k. The influence of the field values, computed using the FVTD technique on the FVTD element facet S_k, on to the resulting field at point $\mathbf{r}$ on Σ can be computed with the second-order accuracy as

$$\begin{aligned}\mathbf{E}(t,\mathbf{r}) = \sum_k \mu(S_k)\frac{\theta(t-\tau_k)}{4\pi R_k}\{\hat{\mathbf{n}}_k \times [\mathbf{E}_k + \tau_k \partial_t \mathbf{E}_k] \times \mathbf{R}_k \\ + (\hat{\mathbf{n}}_k \cdot [\mathbf{E}_k + \tau_k \partial_t \mathbf{E}_k])\mathbf{R}_k\} - \hat{\mathbf{n}}_k \times [\mu_0 \partial_t \mathbf{H}_k]\,\mathrm{d}S \\ \mathbf{H}(t,\mathbf{r}) = \sum_k \mu(S_k)\frac{\theta(t-\tau_k)}{4\pi R_k}\{\hat{\mathbf{n}}_k \times [\mathbf{H}_k + \tau_k \partial_t \mathbf{H}_k] \times \mathbf{R}_k \\ + (\hat{\mathbf{n}}_k \cdot [\mathbf{H}_k + \tau_k \partial_t \mathbf{H}_k])\mathbf{R}_k\}(+\hat{\mathbf{n}}_k \times [\varepsilon_0 \partial_t \mathbf{E}_k])\,\mathrm{d}S \end{aligned} \tag{24}$$

Here, denoting $\mathbf{s}_k$ as the position vector of the barycentre of the surface element S_k, $R_k = |\mathbf{r} - \mathbf{s}_k|$, $\mathbf{R}_k = (\mathbf{r} - \mathbf{s}_k)/R_k^2$, the retarded time for the facet of interest is $\tau_k = R_k/c$, $[\mathbf{E}_k] = \mathbf{E}(t - \tau_k, \mathbf{s}_k)$ and $[\mathbf{H}_k] = \mathbf{H}(t - \tau_k, \mathbf{s}_k)$. In these expressions, $\hat{\mathbf{n}}_k$ is the outward normal to facet S_k having area $\mu(S_k)$, and the values at the barycenters $\boldsymbol{s}_k$ of the facets of S are obtained with the same order of interpolation as used for the flux approximation in the FVTD scheme. This approximation is second-order accurate because field values on each S_k are computed at the barycentre of the facet. In order to utilize the benefits of the IE solution on the mesh boundary we must make appropriate use of it in conjunction with the finite-volume update scheme. We have found using numerical experimentation, that only the incoming flux values should be calculated using the IE, otherwise numerical oscillations occur in the resulting solution. This will now be explained.

Consider a volumetric element T_i for which one of its facets $T_i(k_0)$ belongs to the surface Σ bounding the computational domain. We assume that the integration surface S, containing all sources and inhomogeneities, is far enough from the exterior surface Σ that element T_i lies in free space and all elements 'near' T_i are subject to the same electrical properties as T_i (where 'near' implies all elements used in an interpolatory stencil for updating). For spatial approximations we can approximate volumetric integrals as a sum of surface integrals using Stoke's theorem:

$$\frac{1}{V_i}\int_{T_i} \begin{bmatrix} -\nabla \times \mathbf{H} \\ \nabla \times \mathbf{E} \end{bmatrix} \mathrm{d}\mathbf{x} = \frac{1}{V_i}\sum_{k=1}^{n_i} \int_{T_i(k)} \begin{bmatrix} -\hat{\mathbf{n}} \times \mathbf{H} \\ \hat{\mathbf{n}} \times \mathbf{E} \end{bmatrix} \mathrm{d}\mathbf{s} \tag{25}$$

There are two obvious ways of using IE solution at the barycentre of $T_i(k_0)$ to update the field values in T_i. First, we can compute the solution using flux splitting for all facets except the

DOI: 10.1002/jnm

boundary facet $T_i(k_0)$ (the latter cannot be computed in the usual manner since at $T_i(k_0)$ we do not have knowledge of a solution $\mathbf{u}^{**}$ which depends on the field outside the computational domain). Then, we can use IE to compute the value $\mathbf{u}^{**} = \mathbf{u}^{\text{int}}$ at the barycentre of facet $T_i(k_0)$ and therefore use $\mathbf{u}^{\text{int}}$ to compute the incoming flux from outside the computational domain. Using this technique, a general formulation for computing (25) for all elements in the mesh (boundary or otherwise) may be written as

$$\frac{1}{V_i}\int_{T_i}\begin{bmatrix} -\nabla\times\mathbf{H} \\ \nabla\times\mathbf{E}\end{bmatrix}\mathrm{d}\mathbf{x} = \frac{1}{V_i}\sum_{k=1}^{n_i}\int_{T_i(k)}(\mathbf{A}^{+}(\hat{\mathbf{n}}_k)\mathbf{u}^{*} + \mathbf{A}^{-}(\hat{\mathbf{n}}_k)\{(1-\delta_{k_0}^{k})\mathbf{u}^{**} + \delta_{k_0}^{k}\mathbf{u}^{\text{int}}\})\,\mathrm{d}\mathbf{s} \quad (26)$$

A second, and somewhat simpler approach would be to compute the field $\mathbf{u}^{\text{int}}$ at the barycentre of the boundary facet $T_i(k_0)$ and use that field value for computing both the incoming and outgoing fluxes. In this case, the computation of (25) becomes

$$\frac{1}{V_i}\int_{T_i}\begin{bmatrix} -\nabla\times\mathbf{H} \\ \nabla\times\mathbf{E}\end{bmatrix}\mathrm{d}\mathbf{x} = \frac{1}{V_i}\sum_{k=1}^{n_i}\int_{T_i(k)}(\mathbf{A}^{+}(\hat{\mathbf{n}}_k) + \mathbf{A}^{-}(\hat{\mathbf{n}}_k))\mathbf{u}^{\text{int}}\,\mathrm{d}\mathbf{s} \quad (27)$$

This second approach, although easier, has the drawback that it does not enforce consistency between the IE solution and the solution computed using the usual finite-volume methods (i.e. at the boundary the two solutions are more-or-less independent). We have found that this second approach is not quite as good as the first: numerical oscillations arise in the solution. Thus, results will be given using only the first method.

To use IE (23) to compute field values on the surface Σ we must know the field values at the appropriate retarded times on the surface S. There are several ways to represent the surface S in the computational domain. The most basic (and the one we have adopted) is to choose the surface S such that it coincides with the facets of volumetric elements. Also, it is beneficial to make the surface S as small as possible so as to limit the computational requirements for computing the IE. Because S is selected to coincide with element facets, we must compute the solution at the barycentres of each facet on S. To do so, we use the same interpolation techniques (19) that we have previously used for flux approximations. We note that there are many ways of picking the stencils for computing the field values on S. As it is our desire to compute field values external to S from IE (23), for consistency it may be desirable to select a stencil with more points external to S than internal to S. This is shown in Figure 2. This concern

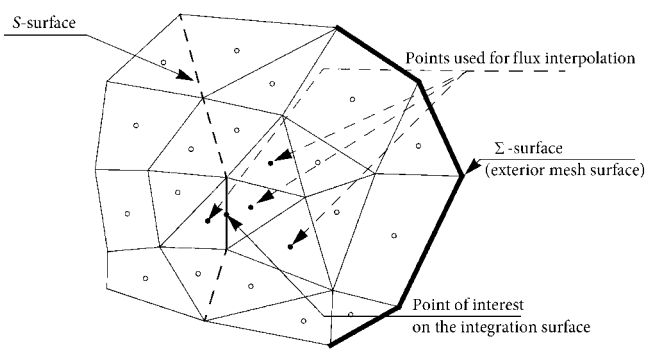

Figure 2. Interpolation on the integration surface S.

DOI: 10.1002/jnm

arises only for higher-order flux interpolation schemes [7] which we are not considering in this paper.

For a surface S comprising of m facets, and a surface Σ composed of n facets, the computation of the boundary values using IE (23) scales as $O(mn)$. For large problems, if m approaches n we have the undesirable computational complexity of $O(n^2)$ at each time step. Fortunately, if this complexity becomes too expensive, it would be possible to apply some sort of fast multipole method [11] to the time-domain IE computation which would reduce the complexity to $O(n \log n)$ or $O(n)$. Details of this approach are beyond the scope of this paper, but we have included their mention for the possibility of future improvements.

5. NUMERICAL RESULTS

5.1. Transient scattering from a PEC sphere

We present the FVTD results for calculating the electromagnetic scattering from a PEC sphere. The reason why we use this as the test case is that an exact eigenfunction solution, the Mie series, is available in the frequency domain, and time-domain waveforms are easily obtained using the inverse Fourier transform. This problem was also selected as a benchmark for the investigation of different high-order interpolation schemes for our FVTD engine [7]. In the present case, the FVTD algorithm we choose to couple with the IE truncation scheme uses the second-order MUSCL-type scheme for spatial approximation and the predictor–corrector scheme for time integration. We also show results of using the second-order MUSCL-type scheme with the second-order absorbing boundary condition applied on the surface of a large sphere which terminates the boundary.

This first case consists of a PEC sphere having a 3-m radius centred in our computational domain. The incident wave is an x-polarized electric field plane-wave transient pulse (see Figure 3). The time variation of the transient pulse, $g(t)$, is chosen as the derivative of a Gaussian:

$$g(t) = \frac{2A(t_0 - t)}{b^2} \mathrm{e}^{-((t-t_0)/b)^2} \theta(t) \tag{28}$$

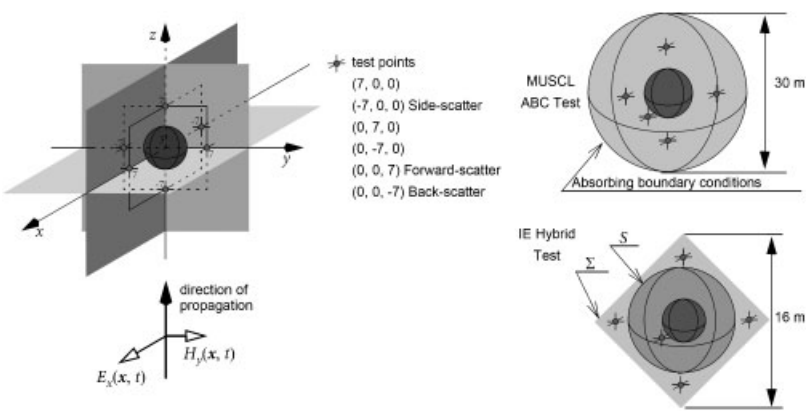

Figure 3. Scattering from a PEC sphere: location of test points and computational domain geometries for (i) the MUSCL and ABC test and (ii) the integral equation hybrid test cases.

DOI: 10.1002/jnm

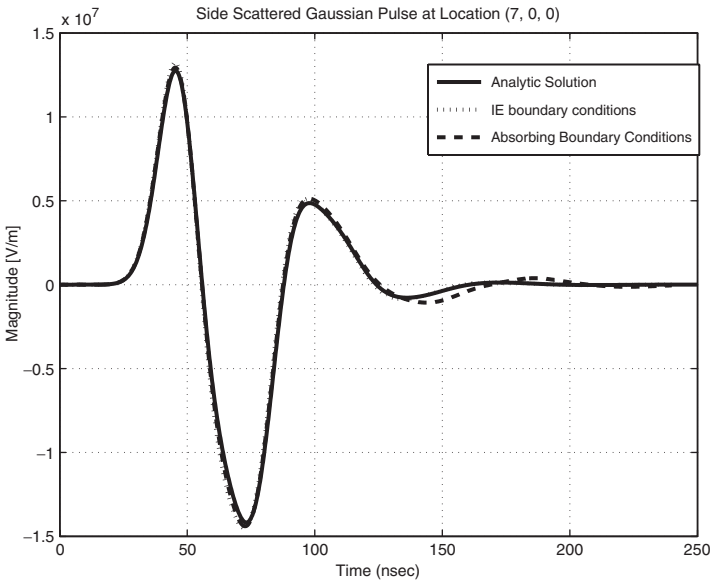

Figure 4. Computational results. E_x at the side-scatter point $(7, 0, 0)$.

with the parameters selected as $A = 1, b = 1.14 \times 10^{-8}$ s and $t_0 = 4.0 \times 10^{-8}$ s. This results in significant energy at the free-space wavelength of about 3 m, i.e. in the resonance region of the sphere. The field quantities, **u**, were computed at those test points shown in Figure 3. For the case of local MUSCL-absorbing boundary conditions, the PEC sphere was put inside a free space spherical mesh having a radius of 15 m to avoid large reflections from the boundary. This large mesh was required to achieve reasonable results using only second-order local boundary conditions.

For the case of IE hybrid technique, a mesh with a cubical outer boundary was chosen. The integration surface was chosen as a sphere of 5 m radius and the Σ surface cube had a diagonal length of only 16 m (see Figure 3).

The computational results for the most difficult case of side-scattering point $(7, 0, 0)$ are shown in Figure 4. The mesh that was used was an unstructured tetrahedral mesh with an average edge length of 0.75 m. The results were found to be in excellent agreement with the exact solution for all three electric field components and for several test-point locations which were tried. Note that the side-scatter point is also the closest to the corner of the cubical outside mesh boundary. Typically, when using local absorbing boundary conditions, such a point would receive a large amount of numerical reflections. The IE technique does not show much difference between points located close to corners of the outside mesh boundary and those located near smoother parts of the outside boundary. Using a laptop computer the simple ABS solution required approximately 30 min whereas the IE-based solution required approximately 3 h.

5.2. *Transient scattering from two PEC cubes*

To demonstrate the potential of the hybrid FVTD/IE method we show results for the transient scattering from two identical PEC cubes. Three cases are considered: (i) using the standard

DOI: 10.1002/jnm

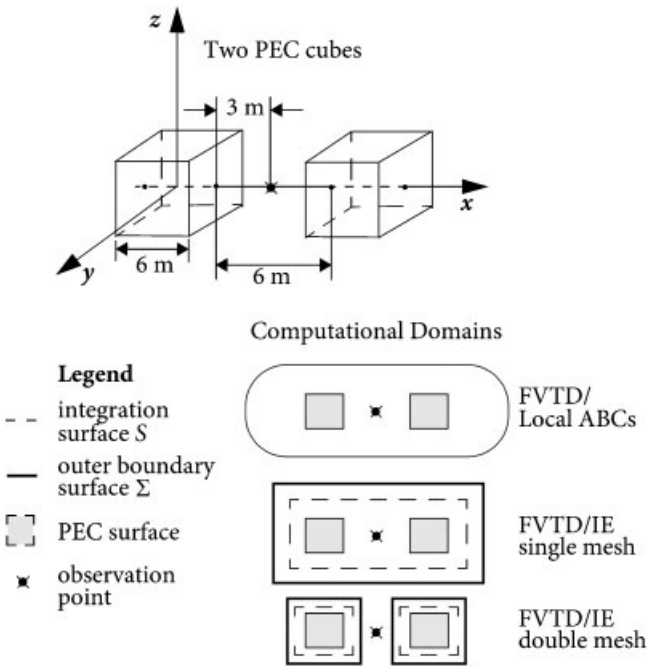

Figure 5. Transient scattering from two PEC cubes; three mesh cases.

FVTD with both cubes inside a single mesh, with second-order absorbing boundary conditions applied at a large distance from the scatterers, (ii) using the FVTD/IE algorithm with a single integration surface S and a single exterior boundary Σ contained both cubes, and (iii) a second FVTD/IE case wherein each cube is contained inside its own FVTD mesh with its own S and Σ surfaces. These are depicted in Figure 5.

The edges of each cube measure 6 m in length and the distance between the centres of the cubes is 12 m. The incident plane wave electromagnetic field is propagated along the x-direction. The time variation of plane wave is the same as for the PEC sphere example. Note, that in case (iii) the field coupling between the two cubes is modelled by the IE and that although there are two S and Σ surfaces, a single update algorithm is implemented: for each point on either Σ surface the IE must be evaluated on both S surfaces. This gives an accurate formulation of the coupling between the two PEC cubes. Energy is propagated from one domain to the other *via* the IE boundary conditions.

The observation point was taken between PEC cubes as shown in the figure. Because the observation point was not located exactly at a finite-volume barycentre, the field at the observation point was computed with the same interpolation procedure as was used for approximating the field at the facet centres. For case (ii), where a single FVTD/IE mesh was used, the IE was used to obtain the field value at the observation point. The results of the computations showed good agreement for all three cases and are shown in Figure 6.

Several other cases, not shown here, indicate that we can use the IE boundary conditions even to compute fields at observation points outside of the computational domain and

DOI: 10.1002/jnm

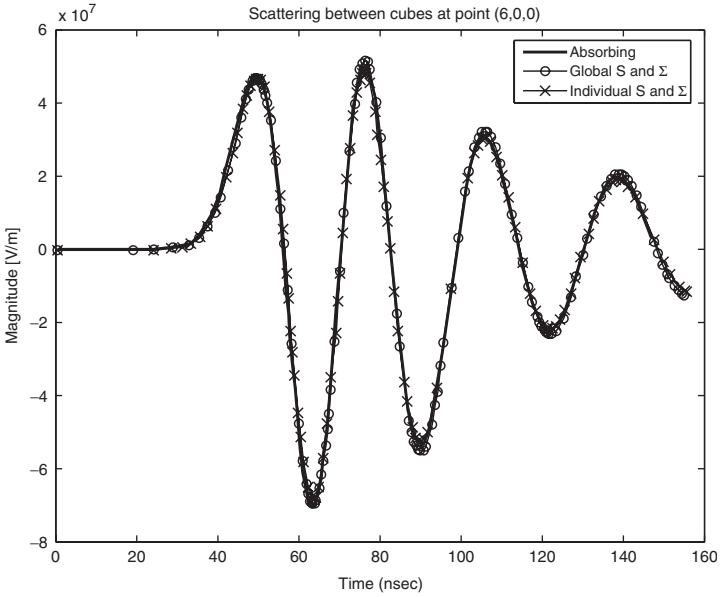

Figure 6. Two PEC cube and an E_z component of the scattered field.

that the interaction between isolated computational subdomains are accurately modelled. No late-time instabilities were present in any of the test cases that we have run to date. We have also found that the outer boundary can be placed almost arbitrarily close to the scatterer without loss of much accuracy, but we have not quantified the effects on numerical accuracy when this is done.

As with the previous example the IE solution took more time to compute. Using a laptop computer the simple ABS solution required approximately 40 min whereas the IE-based solution required approximately 5 h.

6. CONCLUSIONS

We have shown that using a time-domain IE as a boundary condition for the FVTD scheme provides excellent results. The agreement with the analytic solution is almost perfect for scattering from a PEC sphere and using a second-order absorbing boundary condition would require a much larger FVTD mesh. The three main advantages of our hybrid FVTD/IE method are that (1) it allows geometrical objects to be located arbitrarily close to the mesh boundaries without compromising the physics of the problem, (2) it couples the physics of unconnected meshes so that distant scatterers can be surrounded by their own local mesh, thus reducing total mesh size, and (3) the same IE formulation can be used to compute electromagnetic field values at points outside the mesh. Although we have not described the numerical integration in detail, it is obvious that the integral requires a convolution-type time integration. This requires that field components on the integration surface be stored for the whole computation time.

DOI: 10.1002/jnm

Currently, the IE computations take an appreciably longer time than running the simple absorbing boundary conditions but we are currently investigating methods of reducing the storage requirements and speeding up the algorithm. This will be the topic of a future paper. The purpose of this paper was to show the achievable accuracy using the method.

ACKNOWLEDGEMENTS

The authors would like to acknowledge the support of Defence Research and Development Canada and NSERC in performing this research.

REFERENCES

1. Taflove A (ed.). *Advances in Computational Electrodynamics*: *The Finite-difference Time-domain Method*. Artech House Inc.: Boston, MA, 1998.
2. Hirsch C. *Numerical Computation of Internal and External Flows*, *Vol. I*: *Fundamentals of Numerical Discretization*. Wiley: New York, 1988.
3. Bonnet P, Ferrieres X, Michielsen BL, Klotz P, Roumiguières JL. Finite-volume time domain method. In *Time Domain Electromagnetics*, Rao SM (ed.). Academic Press: San Diego, CA, 1999.
4. Fumeaux C, Baumann D, Leuchtmann P, Vahldieck R. A generalized local time-step scheme for efficient FVTD simulations in strongly inhomogeneous meshes. *IEEE Transactions on MTT* 2004; **52**(3):1067–1076.
5. van Leer B. Towards the ultimate conservative difference scheme V. A second order sequel to Godunov's method. *Journal of Computational Physics* 1979; **32**:101–136.
6. Hubbard ME. Multidimensional slope limiters for MUSCL-type finite volume schemes on unstructured grids. *Journal of Computational Physics* 1999; **155**:54–74.
7. Firsov D, LoVetri J, Jeffrey I, Okhmatovski V, Chamma W. High-order FVTD on unstructured grids. *ACES 2006*, *The 22th Annual Review of Progress in Applied CEM*, Miami, FL, 12–16 March 2006.
8. Firsov D, LoVetri J, Jeffrey I, Okhmatovski V, Gilmore C, Chamma W. High-order FVTD on unstructured grids using an object-oriented computational engine. *ACES Journal* 2007; **22**:71–82.
9. Firsov D, LoVetri J. Necessary stability criterion for unstructured mesh upwinding FVTD schemes for Maxwell's equations. *ACES 2007*, *The 23th Annual Review of Progress in Applied CEM*, Verona, Italy, 19–23 March 2007.
10. Ziolkowski RW, Madsen NK, Carpenter RC. Three-dimensional computer modeling of electromagnetic fields: a global lookback lattice scheme. *Journal of Computational Physics* 1983; **50**:360–408.
11. Ergin A, Shanker B, Michielssen E. The plane-wave time-domain algorithm for the fast analysis of transient wave phenomena. *IEEE Antennas and Propagation Magazine* 1999; **41**(4):31–52.
12. Ollivier-Gooch CF. Quasi-ENO schemes for unstructured meshes based on unlimited data-dependent least-squares reconstruction. *Journal of Computational Physics* 1997; **133**(1):6–17.

AUTHORS' BIOGRAPHIES

Dmitry K. Firsov received his diploma (with distinction) and Candidate of Science (PhD) degrees in mathematics from Tomsk State University, Russia, in 1999 and 2002, respectively. In 2002, he was an Assistant Professor at Tomsk State University, Department of Theoretical Mechanics. From 2003 to 2005 he was a post-doctoral fellow with the Department of Mathematics at the University of Manitoba, Canada. Currently, Dmitry is a post-doctoral fellow with the Department of Electrical Engineering at the University of Manitoba. He is currently working in the area of numerical methods for partial differential equations.

DOI: 10.1002/jnm

Joe LoVetri received the PhD degree in electrical engineering from the University of Ottawa, Ont., Canada, in 1991. From 1991 to 1999, he was an Associate Professor in the Department of Electrical and Computer Engineering, University of Western Ontario, Canada. He is currently a Professor in the Department of Electrical and Computer Engineering, and Associate Dean (Research) of the Faculty of Engineering at University of Manitoba, Winnipeg, Canada. His main research interests are in time-domain CEM, modelling of EMC problems, GPR, and inverse imaging techniques.

DOI: 10.1002/jnm